

# Attoclock reveals natural coordinates of the laser-induced tunnelling current flow in atoms

Adrian N. Pfeiffer<sup>1\*</sup>, Claudio Cirelli<sup>1</sup>, Mathias Smolarski<sup>1</sup>, Darko Dimitrovski<sup>2\*</sup>, Mahmoud Abu-samha<sup>2</sup>, Lars Bojer Madsen<sup>2</sup> and Ursula Keller<sup>1</sup>

**In the research area of strong-laser-field interactions and attosecond science<sup>1</sup>, tunnelling of an electron through the barrier formed by the electric field of the laser and the atomic potential is typically assumed to be the initial key process that triggers subsequent dynamics<sup>1–3</sup>. Here we use the attoclock technique<sup>4</sup> to obtain experimental information about the electron tunnelling geometry (the natural coordinates of the tunnelling current flow) and exit point. We confirm vanishing tunnelling delay time, show the importance of the inclusion of Stark shifts<sup>5,6</sup> and report on multi-electron effects clearly identified by comparing results in argon and helium atoms. Our combined theory and experiment allows us to single out the geometry of the inherently one-dimensional tunnelling problem, through an asymptotic separation of the full three-dimensional problem. Our findings have implications for laser tunnel ionization in all atoms and in particular in larger molecular systems with correspondingly larger dipoles and polarizabilities.**

One of the most striking manifestations of the rules of quantum mechanics is the possibility for a particle to move from one side of a potential barrier to the other regardless of the energy height of that barrier. This includes the classically forbidden case, referred to as tunnelling, where the potential energy of the barrier is higher than the energy of the particle (Fig. 1a). In linearly polarized laser fields, electron tunnelling is expected to eventually lead to above-threshold ionization, enhanced double ionization and coherent emission up to the X-ray regime with high-order harmonic generation<sup>7–10</sup>. Therefore, a detailed understanding of the tunnelling step is of paramount importance for attosecond science, including generation of attosecond pulses<sup>11,12</sup> and attosecond measurement techniques<sup>4,13,14</sup>.

The attoclock<sup>4</sup> is an attosecond streaking technique<sup>13</sup>. The rotating electric field vector of a close-to-circularly polarized laser field gives the time reference, in a manner similar to the hands of a clock, and the time is measured by counting fractions of cycles with the exact angular position of the rotating electric field. In this way it is possible to obtain attosecond time resolution by employing a femtosecond pulse. The attoclock was used to set an upper limit to the tunnelling delay time during the tunnel ionization process in helium<sup>15</sup>, and to measure the ionization times in double ionization of argon<sup>16,17</sup>. For the attoclock, a very short few-femtosecond pulse is used to both ionize an atom and to provide the time reference. The pulse duration is kept sufficiently short such that the ionization event is limited to within one optical cycle around the peak of the pulse. As a result of the close-to-circular polarization, re-scattering of the liberated electron with the parent ion is mostly suppressed. Assuming classical

propagation of the liberated electron, the instant of ionization can be mapped to the angle of the final momentum of the electron in the polarization plane, measured with cold target recoil ion momentum spectroscopy<sup>18</sup> (Fig. 2).

Here, we use the attoclock to measure the offset angle  $\theta$  (defined in Fig. 3) that is directly related to the complex parent ion interaction and therefore extremely sensitive to the exact tunnel geometry. The attoclock cycle, the time zero (that is, the direction of the maximum laser field vector) and the exact time evolution of the streaking laser field are fully characterized independently (Supplementary Information). We minimize systematic errors in the angular streaking using both clockwise and anticlockwise polarized pulses (Fig. 3). The ionization event remains the same, but the clockwise and anticlockwise laser fields will streak the electron at the exit of the tunnel by equal amounts but in opposite directions.

In the experiments, we vary the peak intensity and therefore the Keldysh parameter<sup>19</sup> from 0.5 to 1.1 and to 1.4 for helium and argon, respectively. Figure 4 shows the angular shift  $\theta$  due to the interaction with the ionic potential during the angular streaking, as explained in Fig. 3. No significant intensity dependence of  $\theta$  is observed for helium over the investigated intensity range (Fig. 4c), whereas argon exhibits a monotonic downwards trend of  $\theta$  with increasing intensity (Fig. 4b).

Time-dependent Schrödinger equation (TDSE) simulations<sup>20</sup> (Fig. 4b) could be carried out only for three peak intensities without serious numerical problems (Supplementary Information). The TDSE results refer to a calculation employing a shorter pulse than the experimental one (a pulse of duration of three cycles as opposed to three cycles in full-width at half-maximum of the intensity, employed in the experiment). Volume effects, not included in the TDSE results, would result in larger angular shifts compared with considering only the peak intensity. We use a semiclassical tunnelling model, TIPIS (tunnel ionization in parabolic coordinates with induced dipole and Stark shift; Fig. 4), that consists of an initial tunnelling step and subsequent classical propagation of the electron trajectory starting at the tunnel exit point (Fig. 1). The offset angle is especially sensitive to the ion–electron interaction and the tunnel exit point: the attraction to the ion at the beginning of the electron trajectory is reflected in an angular offset  $\theta$  when compared with the laser-only trajectory (Figs 2b and 3). Without the forces from the parent ion the angular offset  $\theta$  would be zero<sup>15,20</sup>, and the final momentum would then be given by the integral of the electric field from the instant of ionization  $t_0$ ; that is, the final momentum would follow the vector potential  $\mathbf{A}(t_0)$  (ref. 21). Even without considering the effect of the ionic potential, any tunnelling delay time  $\Delta t_D$  will manifest itself as an angular

<sup>1</sup>Physics Department, ETH Zurich, 8093 Zurich, Switzerland, <sup>2</sup>Lundbeck Foundation Theoretical Center for Quantum System Research, Department of Physics and Astronomy, Aarhus University, 8000 Aarhus C, Denmark. \*e-mail: apfeiff@phys.ethz.ch; darkod@phys.au.dk.

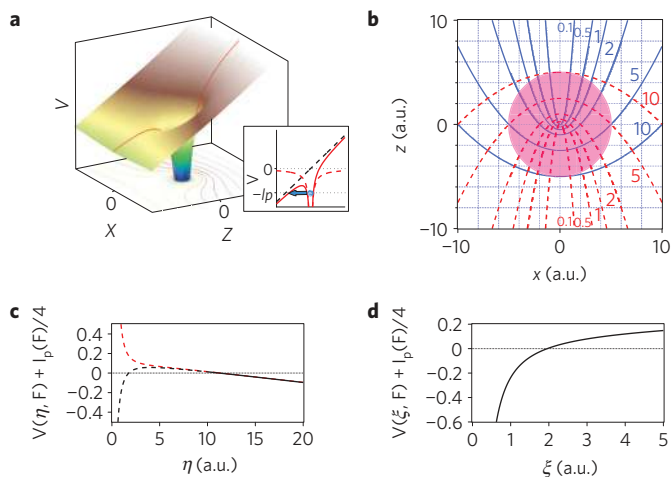


**Figure 1 | Strong-field tunnelling.** Laser-induced adiabatic tunnelling picture<sup>19,29</sup> where the laser frequency is much smaller than the oscillation frequency of the bound-state electron. Our helium and argon experiments in the near-infrared region fulfil this approximation (see Supplementary Information). This means that the combined 3D potential field of the ion and laser shown in **a** for  $y = 0$  changes slowly. The only escape is then through tunnelling and a quasi-static potential barrier can be used. **a**, The field  $F$  is assumed to be pointing in the positive  $z$  direction. A cut of the potential along the instantaneous field direction, along  $z$  and for  $x = 0$  gives the field-direction model as given by the inset. **b**, Illustration of parabolic coordinates that separate the Schrödinger equation for the electron in the combined Coulomb and laser potentials. The figure shows a cut for  $y = 0$  and the red dashed curves correspond to contours with constant  $\xi$ , and the blue curves correspond to contours with constant  $\eta$ ; the values of  $\xi$  and  $\eta$  are given next to the contours. The magenta circle illustrates the approximate region in position space where the exact atomic potential is non-separable in parabolic coordinates and where the far-field expression for the dipole terms (equation (2)) cannot be used. In **b** we see that when we vary  $\eta$ , the coordinate in which tunnelling occurs (see **c**), many values of  $x$  and  $z$  are probed and this effect obtained in the parabolic coordinates that separate the Schrödinger equation is not captured by the field-direction model. **c,d**, The effective potential plus the binding energy for argon at the experimental intensity of  $5 \times 10^{14} \text{ W cm}^{-2}$  along  $\eta$  (**c**) and along  $\xi$  (**d**). The potential  $V(\eta, F)$  has a barrier through which the electron may tunnel, whereas the potential  $V(\xi, F)$  does not form a barrier and there is no possibility for the electron to escape by tunnelling. The approximate expectation value of  $\xi$  for the wavefunction bound in  $V(\xi, F)$  is 1. With this expectation value of  $\xi$ , the solid line in **c** starting at  $\eta = 10$  a.u. corresponds to  $\xi/\eta \ll 1$ . In this region separation in parabolic coordinates is possible and this is where the tunnel exit point is located. The dashed curves give the potential in the inner, non-separable region where we assume that the potential forms a barrier. The red dashed line corresponds to the potential (2), and the black dashed line corresponds to the same potential with the induced dipole term multiplied with  $\exp(-3/\eta)$  to account for the fact that pure dipole-like potential can be used only in the far field.

offset, because instead of  $-\mathbf{A}(t_0)$ , the final momentum would then be  $-\mathbf{A}(t_0 - \Delta t_D)$ . The offset angle is extremely sensitive to the tunnelling delay time, with one degree in  $\theta$  corresponding to  $\Delta t_D \approx 5\text{--}10$  as. The excellent agreement of our theory for both atoms and over a large intensity range below and above the Keldysh parameter  $\gamma = 1$  confirms zero tunnelling time within the experimental accuracy of 10 as.

Although the electron feels the full three-dimensional (3D) potential (Fig. 1a), only the potential in the direction of the field is usually considered<sup>22</sup>. We will refer to this model as the ‘field-direction model’. Using that model, one can predict that

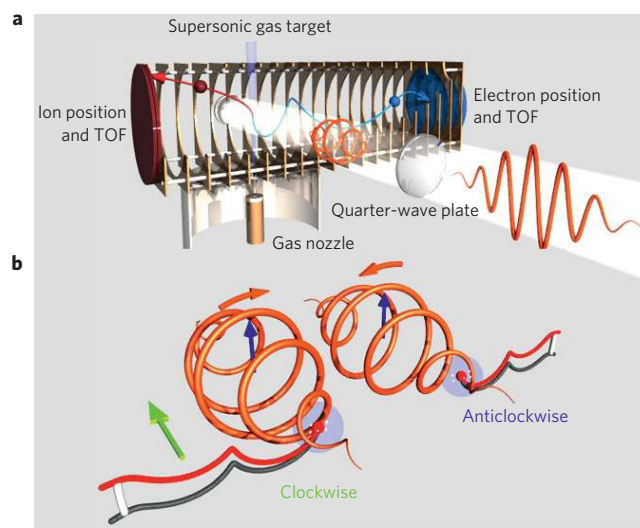


**Figure 2 | Attoclock principle.** **a**, Attoclock<sup>4,15</sup> set-up with a cold target recoil ion momentum spectrometer<sup>18</sup>. An intense infrared laser pulse (about 3 cycles, 7 fs pulse duration, centre wavelength 740 nm, 1 kHz pulse repetition rate) from a Ti:sapphire laser system with a two-stage filament compressor<sup>30</sup> is propagated through a quarter-wave plate to produce a close-to-circularly (ellipticity 0.78) polarized laser field. The rotating electric field vector gives the time reference, in a manner similar to the hands of a clock. This pulse is then focused into a supersonic gas target to tunnel-ionize helium or argon. The ions and electrons are guided onto time- and position-sensitive detectors, to determine, in coincidence, the momenta of the atomic fragments after the laser pulse. Much less than one ionization event occurs per pulse. TOF, time of flight. **b**, Angular streaking with both clockwise and anticlockwise close-to-circular polarization. The green arrow illustrates the laser propagation direction and the blue arrow represents the rotating electric field vector (that is, the hand of the attoclock) at peak intensity. The time evolution of the peak of the electric field vector is shown in orange for both clockwise and anticlockwise polarization. The tunnelling delay time<sup>15</sup> is defined by the angular difference between the maximum of the electric laser field (blue arrow), which induces the highest tunnelling ionization rate, and the direction of the laser field when the electron exits the tunnel. At the exit of the tunnel, the electron is assumed to be in the continuum and to experience the acceleration of the strong laser field present at that moment. Depicted are electron trajectories<sup>21</sup> in red and black, with and without the interaction with the parent ion respectively, which then determine the momenta at the target after the pulse (**a**).

over-the-barrier ionization (OBI) occurs for argon within the intensity range investigated in this work. The comparison between theory and experiment (Fig. 4b,c) shows that the calculation based on tunnel exit points obtained from the field-direction model fails to reproduce the experimental trend in  $\theta$ , the curves exhibiting a non-monotonic dependence on laser intensity by having a pronounced local maximum close to the OBI intensity (Fig. 4b). The reason is that for the problem at hand the direction along the field is non-separable.

A separation of the Schrödinger equation for the electron in the external field is possible for the pure Coulomb problem in parabolic coordinates  $\xi = r + z$  and  $\eta = r - z$  (see Fig. 1b). In that case, the resulting one-dimensionality of the separated problem enables an analytical treatment of tunnelling<sup>23</sup>. Here we consider multi-electron systems, and show that a separation of the problem is still possible for relevant  $\xi$  and  $\eta$  values. In the inner region (Fig. 1b,c), we do not know the potential, but our procedure to determine the exit points is not sensitive to this lack of knowledge, as the region of space where the exit points are is separable in

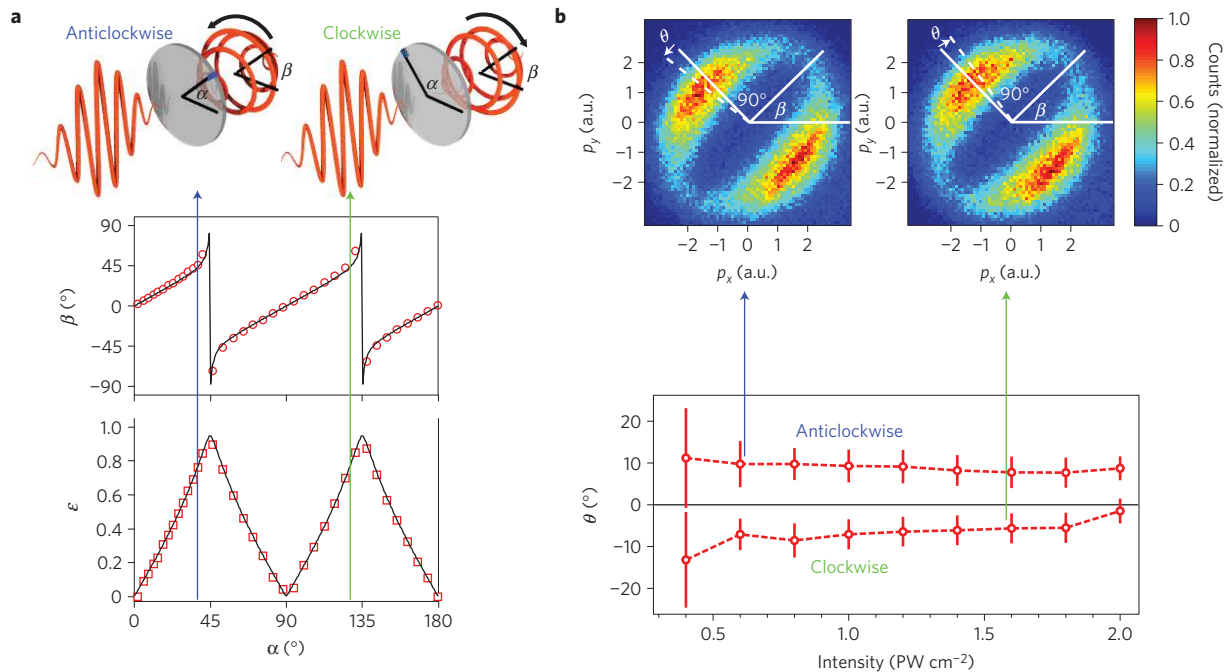


**Figure 3 | Systematic error reduction in angular streaking.** Applying both clockwise and anticlockwise polarization under the same experimental conditions minimizes systematic errors with the attoclock. The dynamics of the tunnel ionization event is preserved; the clockwise and anticlockwise field will streak the electron at the exit of the tunnel by equal amounts but in opposite directions. **a**, The angle  $\alpha$  between the fast axis of a quarter-wave plate and the polarization plane of the incoming laser pulse determines the ellipticity  $\epsilon$  and the angle of the polarization ellipse  $\beta$ . The measurement (red) is in excellent agreement with the simulation (black)<sup>21</sup>. For two angles  $\alpha$  separated by  $90^\circ$ , the polarization is identical, except for the turning direction of the electric field vector. **b**, The ion momentum distribution peak (dashed white line) rotated by  $90^\circ$ —compared with the major polarization axis at angle  $\beta$  due to the propagation in the laser field alone<sup>21</sup>. An additional angular offset  $\theta$  into the electric field turning direction is observed due to the interaction with the ion. The intensity dependence of  $\theta$  is shown in the lower graph for anticlockwise and clockwise turning fields. The error bars show the standard deviation of a double Gaussian fit that extracts  $\theta$  from the radially integrated ion momentum distribution (see ref. 4 for details). For all of our results as presented in Fig. 4, we considered both measurements from anticlockwise and clockwise (with a sign change in  $\theta$ ) streaking fields. Wavelength and pulse duration are given in the caption of Fig. 2.

parabolic coordinates (Fig. 1c). Our procedure reveals the universal tunnelling geometry for atoms.

The complete derivation of our model is given in the Supplementary Information; here we provide only a sketch. In a static field  $\mathbf{F}$ , we use the adiabatic approximation to find the effective potential<sup>24</sup> for the outer electron, including the field and the multi-electron effects<sup>5</sup> (atomic units are used),

$$V_{\text{ef}}(\mathbf{r}, \mathbf{F}) = -\frac{1}{r} - \frac{\alpha^I \mathbf{F} \cdot \mathbf{r}}{r^3} + \mathbf{F} \cdot \mathbf{r} \quad (1)$$

where  $\alpha^I$  is the static polarizability of the ion. Then, we carry out an approximate separation of the one-electron problem in a potential (1) in parabolic coordinates in the limit  $\xi/\eta \ll 1$  (satisfied for the present experiment). The obtained effective potential along the  $\eta$  coordinate (the coordinate through which tunnelling occurs) is

$$V(\eta, F) = -\frac{(1 - \sqrt{2I_p(F)}/2)}{2\eta} - \frac{1}{8}\eta F + \frac{m^2 - 1}{8\eta^2} + \frac{\alpha^I F}{\eta^2} \quad (2)$$

where  $I_p(F) = I_p(0) + 1/2(\alpha^N - \alpha^I)F^2$  is the Stark-shifted ionization potential<sup>6,25,26</sup> and  $\alpha^N$  is the static polarizability of the atom. We note that the procedure above is not just a change of coordinates, rather another separation procedure that defines a different tunnelling geometry. In the parabolically separated problem, the tunnelling geometry is a line along the parabolic  $\eta$  coordinate but it defines a whole region in the 3D space, whereas in the field-direction model, the tunnelling geometry is a line in a 3D space. The exit points are determined by equating the potential (2) with  $m = 0$

and the energy term  $-I_p(F)/4$ . We note that the induced dipole (polarization) term is not included in the TDSE. The effect of the multi-electron polarization term is small for the intensities at which the TDSE results could be obtained (Fig. 4b).

The tunnel exit points obtained from the separated problem are generally larger than those obtained in the field-direction model<sup>26</sup>, and the inclusion of the Stark shifts (larger binding energy) and induced dipole of the ion (larger barrier) pushes the exit points even farther away from the origin (Fig. 4a). The induced dipole and Stark shifts also lead to an increase of the OBI; however, the experimental parameters are such that in the parabolically separated problem, no OBI occurs (Fig. 4a). As a result of the very small polarizabilities of He and He<sup>+</sup>, the Stark shifts and the induced dipole barrier modification are negligible, and it is the parabolically separated model that leads to a plateau in the  $\theta$  dependence on intensity, rather than the weak monotonic increase produced by the field-direction model (Fig. 4c). For the case of argon, with larger polarizabilities, the inclusion of Stark shifts, and even more, the multi-electron effect through the increase of the barrier due to the induced dipole of the ion, becomes decisive for the decrease of  $\theta$  with increasing intensity (Fig. 4b). The prediction for the trend in  $\theta$  is insensitive to the exact form of the rate, the only requirement being that the rate increases with increasing intensity (Supplementary Information), and that gives further confidence about the calculated exit points in time and space.

The attoclock technique allowed us to gain new insights into laser-induced tunnelling, one of the paradigms of modern strong-field and ultrafast science. We have confirmed vanishingly small tunnelling time and, above all, revealed the natural geometry of

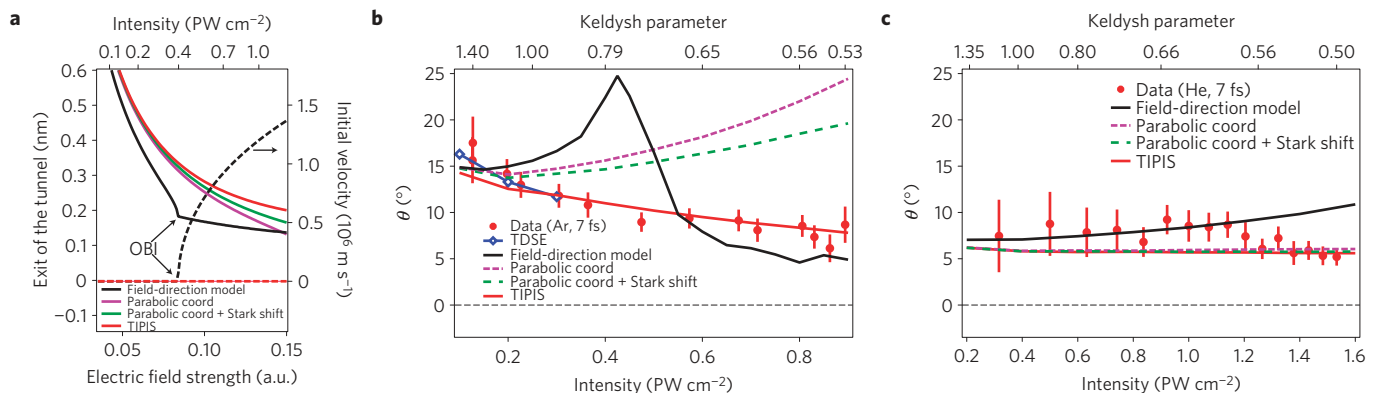


**Figure 4 | Offset angle for argon and helium.** **a**, Exit of the tunnel for argon as a function of electric field strength and laser intensity for different models. If the field-direction model is used, OBI is reached at about  $4 \times 10^{14} \text{ W cm}^{-2}$ . Over this intensity, the electron is placed at the combined potential saddle point with an initial non-zero velocity (dashed line) longitudinal to the electric field at the instant of ionization (Supplementary Information). ‘Parabolic coord’ refers to the parabolically separated model without inclusion of the Stark shifts and multi-electron effects of equation (2); ‘Parabolic + Stark shift’ refers to the problem of equation (2) with inclusion of Stark shifts, but without inclusion of multi-electron effects. ‘TIPIIS’ refers to our full model. **b**, Experimental data of  $\theta$ , obtained from electron momentum distributions in argon, as a function of laser intensity, together with the curves predicted by the TDSE and different models (see Fig. 3 for the estimation of the error bars). For all of the models, the exit of the tunnel and the eventual initial velocity are determined as in **a**. The figure shows that the measured trend is reproduced only when the multi-electron effect due to the polarized ion is included. Wavelength and pulse duration are given in the caption of Fig. 2. **c**, The same as for **b**, but for helium, obtained from ion momentum distributions.

laser-induced tunnelling in atoms, defined by the tunnelling current flow along one parabolic coordinate. Furthermore, our model showed and quantified the contributions of the Stark shifts of the bound-state energy levels and the multi-electron effects describing the action of the induced dipole of the core electrons on the liberated electron. The extent to which the multi-electron effects influence the tunnelling dynamics is system dependent as shown here by the difference in helium and argon. Argon is much easier to polarize than helium and is therefore affected more strongly.

The implications of our study are significant in particular to attosecond science and strong-field physics. First, the intensity range where the electron still emerges below the tunnel barrier is significantly extended towards higher intensities. This is important for new attosecond measurement concepts because the liberated electrons in the laser-induced tunnelling regime exhibit more precisely defined properties and theoretical tools suited for below-the-barrier ionization can be used. Second, the multi-electron effects identified here will greatly affect further studies on larger molecules and on surfaces where much less is known. In particular, larger molecules are much more polarizable than the noble gas atoms studied here, and the effects reported here will be visible especially in experiments employing circularly or near-circularly polarized laser pulses that isolate the ionization event. Third, attosecond measurements typically rely on streaking techniques that are highly sensitive to the parent ion interaction<sup>27,28</sup>, which needs to be described precisely (taking additional force terms such as those identified in the present work) to draw conclusions on the time delays.

Received 20 January 2011; accepted 20 September 2011; published online 23 October 2011

## References

- Krausz, F. & Ivanov, M. Attosecond physics. *Rev. Mod. Phys.* **81**, 163–234 (2009).
- Brabec, T. & Krausz, F. Intense few-cycle laser fields: Frontiers of nonlinear optics. *Rev. Mod. Phys.* **72**, 545–591 (2000).
- Chang, Z. H. & Corkum, P. Attosecond photon sources: The first decade and beyond. *J. Opt. Soc. Am. B* **27**, B9–B17 (2010).
- Eckle, P. *et al.* Attosecond angular streaking. *Nature Phys.* **4**, 565–570 (2008).
- Dimitrovski, D., Martiny, C. P. J. & Madsen, L. B. Strong-field ionization of polar molecules: Stark-shift-corrected strong-field approximation. *Phys. Rev. A* **82**, 053404 (2010).
- Holmgaard, L. *et al.* Photoelectron angular distributions from strong-field ionization of oriented molecules. *Nature Phys.* **6**, 428–432 (2010).
- Corkum, P. B. Plasma perspective on strong-field multiphoton ionization. *Phys. Rev. Lett.* **71**, 1994–1997 (1993).
- McPherson, A. *et al.* Studies of multiphoton production of vacuum-ultraviolet radiation in the rare gases. *J. Opt. Soc. Am. B* **4**, 595–601 (1987).
- L’Huillier, A. & Balcou, P. High-order harmonic generation in rare gases with a 1-ps 1053-nm laser. *Phys. Rev. Lett.* **70**, 774–777 (1993).
- Krause, J. L., Schafer, K. J. & Kulander, K. C. High-order harmonic-generation from atoms and ions in the high-intensity regime. *Phys. Rev. Lett.* **68**, 3535–3538 (1992).
- Paul, P. M. *et al.* Observation of a train of attosecond pulses from high harmonic generation. *Science* **292**, 1689–1692 (2001).
- Hentschel, M. *et al.* Attosecond metrology. *Nature* **414**, 509–513 (2001).
- Kienberger, R. *et al.* Atomic transient recorder. *Nature* **427**, 817–821 (2004).
- Schultze, M. *et al.* Delay in photoemission. *Science* **328**, 1658–1662 (2010).
- Eckle, P. *et al.* Attosecond ionization and tunneling delay time measurements in helium. *Science* **322**, 1525–1529 (2008).
- Pfeiffer, A. N., Cirelli, C., Smolarski, M., Dörner, R. & Keller, U. Timing the release in sequential double ionization. *Nature Phys.* **7**, 428–433 (2011).
- Pfeiffer, A. N. *et al.* Breakdown of the independent electron approximation in sequential double ionization. *New J. Phys.* **13**, 093008 (2011).
- Dörner, R. *et al.* Cold target recoil ion momentum spectroscopy: A ‘momentum microscope’ to view atomic collision dynamics. *Phys. Rep.* **330**, 95–192 (2000).
- Keldysh, L. V. Ionization in the field of a strong electromagnetic wave. *Sov. Phys. JETP* **20**, 1307–1314 (1965).
- Martiny, C. P. J., Abu-samaha, M. & Madsen, L. B. Counterintuitive angular shifts in the photoelectron momentum distribution for atoms in strong few-cycle circularly polarized laser pulses. *J. Phys. B* **42**, 161001 (2009).
- Smolarski, M., Eckle, P., Keller, U. & Dörner, R. Semiclassical model for attosecond angular streaking. *Opt. Express* **18**, 17640–17650 (2010).
- Nubbemeyer, T., Gorling, K., Saenz, A., Eichmann, U. & Sandner, W. Strong-field tunneling without ionization. *Phys. Rev. Lett.* **101**, 233001 (2008).
- Landau, L. D. & Lifschitz, E. M. *Quantum Mechanics (Non-relativistic Theory)* (Oxford Univ. Press, 1958).
- Bhardwaj, V. R., Corkum, P. B. & Rayner, D. M. Internal laser-induced dipole force at work in  $\text{C}_{60}$  molecule. *Phys. Rev. Lett.* **91**, 203004 (2003).
- Lein, M. Streaking analysis of strong-field ionisation. *J. Mod. Opt.* **58**, 1188–1194 (2011).
- Shakeshaft, R., Potvliege, R. M., Dörner, M. & Cooke, W. E. Multiphoton processes in an intense laser field. IV. The static-field limit. *Phys. Rev. A* **42**, 1656–1668 (1990).
- Baggesen, J. C. & Madsen, L. B. Polarization effects in attosecond photoelectron spectroscopy. *Phys. Rev. Lett.* **104**, 043602 (2010).
- Kheifets, A. S. & Ivanov, I. A. Delay in atomic photoionization. *Phys. Rev. Lett.* **105**, 233002 (2010).
- Perelomov, A. M., Popov, V. S. & Terentev, M. V. Ionization of atoms in an alternating electric field. *Sov. Phys. JETP* **23**, 924–934 (1966).

30. Hauri, C. P. *et al.* Generation of intense, carrier-envelope phase-locked few-cycle laser pulses through filamentation. *Appl. Phys. B* **79**, 673–677 (2004).

### Acknowledgements

This work was supported by the NCCR Quantum Photonics (NCCR QP) and NCCR Molecular Ultrafast Science and Technology (NCCR MUST) programmes, research instruments of the Swiss National Science Foundation (SNSF), ETH Research Grant ETH-03 09-2, an SNSF equipment grant and the Danish Council for Independent Research, Natural Sciences.

### Author contributions

A.N.P., C.C., M.S. and U.K. carried out experiments and simulations. D.D., M.A.-s. and L.B.M. developed the theory. All authors participated in the writing of the paper.

### Additional information

The authors declare no competing financial interests. Supplementary information accompanies this paper on [www.nature.com/naturephysics](http://www.nature.com/naturephysics). Reprints and permissions information is available online at <http://www.nature.com/reprints>. Correspondence and requests for materials should be addressed to A.N.P. or D.D.